Journal of Building Engineering 31 (2020) 101336

Contents lists available at ScienceDirect

Journal of Building Engineering

journal homepage: http://www.elsevier.com/locate/jobe

Utilization of size-tunable hollow silica nanospheres for building thermal insulation applications

Sohrab Alex Mofid [a,b,*], Bjørn Petter Jelle [a,d], Xinpeng Zhao [b], Tao Gao [a], Mathieu Grandcolas [f], Bridget Cunningham [c], Serina Ng [d], Ronggui Yang [b]

[a] Norwegian University of Science and Technology (NTNU), Department of Civil and Environmental Engineering, NO-7491, Trondheim, Norway
[b] University of Colorado Boulder (CU-Boulder), Department of Mechanical Engineering, CO-80309, Colorado, USA
[c] University of Vermont (UVM), Department of Art and Art History, VT-05405, Vermont, USA
[d] SINTEF Building and Infrastructure, Department of Materials and Structures, NO-7465, Trondheim, Norway
[f] SINTEF Industry, Department of Materials and Nanotechnology, NO-0373, Oslo, Norway

ARTICLE INFO

Keywords:
Nano insulation material
Hollow silica nanosphere
HSNS
Superinsulation material
Thermal conductivity

ABSTRACT

Hollow silica nanospheres (HSNS) have been the subject of intense studies as a possible building block that may successfully bring about nano insulation materials (NIM) with substantially reduced thermal conductivity. The reported thermal conductivity values of the HSNS are currently ranged between 20 and 90 mW/(mK). In this work, we have investigated the thermal properties of HSNS as a function of the corresponding structural parameters such as inner pore diameter, porosity, shell thickness, and size of the silica nanoparticles constituting the shell of HSNS. HSNS with sizes less than 100 nm was specifically synthesized in an attempt to lower the expressed thermal conductivity values to be below 20 mW/(mK), which may be used as a potential target towards superinsulation materials used in building applications. Furthermore, synthetic approaches to gain insights into the mechanism and formation of HSNS, i.e., the influence of reaction parameters on the structural characteristics of HSNS, have been thoroughly discussed in this work.

1. Introduction

Hollow silica nanospheres (HSNS) have garnered much attention due to their unique properties such as low density, high porosity, large surface area to volume ratio and encapsulating ability [1,2], which have led to significant advances in applications for biomedical, electrical, and construction sectors [3–7]. HSNS may provide noticeable advantages to explore for miscellaneous thermal insulation applications [8]. For example, previous studies have demonstrated thermal insulation properties of HSNS, i.e., a reduced low thermal conductivity of about 20–90 mW/(mK), comparable to that of stagnant air of about 26 mW/(mK) [8–12]. It is intriguing that HSNS may potentially enable a new generation of nano-porous insulation materials with small pore sizes and low volume fraction of solid [13,14].

Distinctive advantages of HSNS for thermal insulation applications are amongst others, their controllability, i, e., thermal properties of HSNS being promptly modified by utilization of their structural characteristics, such as inner pore diameter and shell thickness. In general, HSNS can be classified as an air cavity enclosed by an inorganic shell with tailored structural features, where the voids are usually correlated to the use of sacrificial templates during the synthesis of HSNS [15]. Thus, the inner pore size of HSNS can be readily controlled by using the templates, e.g. polyacrylic acid (PAA) or polystyrene (PS), with different dimensions; the shell thickness of HSNS can be adjusted by a controlled growth and deposition of silica nanoparticles; and the shell morphology, depending on the reaction conditions, may be dense or porous. Therefore, it is possible to capitalize on the apparent structural features of HSNS to tailor their size-dependent thermal insulation properties.

Currently, the lowest reported thermal conductivity values of HSNS are typically of about 20 mW/(mK). For example, Liao et al. reported a thermal conductivity of ~20 mW/(mK) using 3ω method for HSNS powder with a typical inner diameter of ~200 nm and a shell thickness of ~40 nm. Gao et al. (2013) reported a thermal conductivity value of ~20 mW/(mK) using HotDisk measurement for HSNS powder with an inner pore diameter of about ~150 nm and a shell thickness of ~20 nm. Recently Li et al. (2014) presented a theoretical model to analyze the

* Corresponding author. Norwegian University of Science and Technology (NTNU), Department of Civil and Environmental Engineering, NO-7491, Trondheim, Norway.
E-mail address: sohrab.mofid@ntnu.no (S.A. Mofid).

https://doi.org/10.1016/j.jobe.2020.101336
Received 5 May 2019; Received in revised form 1 February 2020; Accepted 4 March 2020
Available online 7 March 2020

parameter variation on the thermal conductivity values of HSNS assemblies. They suggested that HSNS have the potential to reach a thermal conductivity as low as ~10 mW/(mK). Prior studies mostly account for thermal conductivity values of HSNS powder with pore sizes greater than 150 nm. However, the size effect on the thermal conductivity reduction becomes more prominent as the dimension reaches sub-100 nm range [16], where the pore size becomes comparable to the mean free path of the gas molecules (~70 nm, 300 K, 1.0 atm) that may well alter the gaseous thermal conductivity values. The existing 10 mW/(mK) gap between theoretical and experimental values may be bridged by investigating, say, inner pore diameter or shell thickness. However, it remains a significant challenge to experimentally validate the HSNS thermal properties.

The objective of this study is to optimize the thermal performance of HSNS with respect to parameter variations, specifically HSNS with inner pore sizes less than 100 nm, in an attempt to substantially lower the thermal conductivity far below 20 mW/(mK), which may present a less expensive alternative towards superinsulation materials (SIM).

2. Experimental

2.1. Chemicals and materials

Reagent grade styrene (St), polyvinylpyrrolidone (PVP; Mw ≈ 40k Da), potassium sulfate (KPS), ammonium hydroxide (NH_4OH, 28–30 wt %), tetraethyl orthosilicate (TEOS), ethanol (96%) and methanol (99.8%) were purchased from Sigma Aldrich and employed as as-supplied without additional purifications. Monodisperse polystyrene spheres (PS), with mean diameter of 46 nm (SD 5 nm) and 85 nm (SD 2 nm) were purchased from Corpuscular Inc., New York, USA and Micro Particles GmbH, Germany, respectively. The commercial PS spheres were used as received. The mean diameter of the PS purchased from Corpuscular Inc., New York, USA was remeasured using both Hitachi S-5500 SEM and Nanosight-LM10 nanoparticle analysis, and corrected at 79 nm (SD 5 nm) not the original 46 nm advertised by the manufacturer.

2.2. Methodology

Various fabrication methods of HSNS with details can be found from earlier studies [17–24]. In this study, HSNS was formed using the sacrificial-template method as depicted in transmission electron microscope (TEM) images given in Fig. 1. Polystyrene (PS) was used as template for providing the nucleation site for the growth of silica shell, which in theory can be any other material with suitable morphology, such as liquid droplets, solid particles [10] or gas bubbles [11,25]. Given the widespread knowledge that exists within silica-based materials, as well as possessing certain characteristics, e.g. abundance, low-cost, low thermal conductivity, non-flammable and environmentally friendliness of silica, it is considered as one of the best possible candidate materials for achieving the hollow nanospheres for thermal insulation purposes. Tetraethyl orthosilicate (TEOS) was used as the silica precursor to form the shell structure. It is worth to note that other silica source materials such as water glass (Na_2SiO_3) may also be used for successful synthesis of HSNS [24].

2.3. Synthesis of polystyrene templates

Polystyrene (PS) templates were synthesized via an emulsion polymerization process, where the ratio of PVP/St was varied to adjust the size of the obtained PS spheres. For a typical synthesis, 10 g of styrene and desired amount of PVP were homogenized in 100 mL of distilled water at room temperature (RT) for 10 min in a 250 mL Erlenmeyer round flask. The mixture was maintained at a constant temperature of ~70 °C applying a hotplate with heat-on block under stirring conditions of 450 rpm. Chosen KPS amount dissolved in 10 mL of distilled water was then added to the mixture slowly and the reaction solution was kept stirring for 24 h. The obtained PS solutions are designated as PS-size, e.g. PS-90, as shown in Table 1.

2.4. Coating of PS templates with TEOS and subsequent calcination

Tetraethyl orthosilicate (TEOS) was used as the silica precursor to form the shell structure. For a typical synthesis, 8 g of PS solution was dispersed in 140 mL of 96% ethanol at 450 rpm for 15 min. Then 4.5 mL of NH_4OH was added and pH value of the system was maintained at around 11. Afterwards, the mixture was stirred for 15 min. TEOS solution (5 mL TEOS in 5 mL of ethanol) was then added to the Erlenmeyer round flask using a Nexus 3000 syringe pump. Four different infusion pump rates were adopted, i.e. 15, 35, 160, and 450 μl/min. The final mix was left stirring at 450 rpm for 8 h at RT. All the coated PS-silica samples were subjected to centrifugation at 5000 rpm for 15 min, air dried overnight and calcined at 440 °C for 6–8 h (heating rate = 5 °C/min) to remove the PS template cores by calcination.

2.5. Characterization

The commercial Netzsch laser flash apparatus (LFA 457) and Netzsch differential scanning calorimetry (DSC 204 F1 Phoenix) were used for the thermal diffusivity α and the specific heat capacity c_p measurements, respectively. A special sample holder specifically designed for powder samples were used in the measurements. Thermal conductivity λ values of HSNS samples can be calculated by Refs. [26,27]:

Table 1
Obtained PS samples of different sizes as result of varying the PVP/St ratio and KPS amount.

Polystyrene-nm	PVP/Styrene Ratio	KPS	Weight/Volume (Aqueous Solution)
PS-213	0.1334	0.131	22%
PS-150	0.1612	0.142	22%
PS-100	0.1976	0.166	22%
Commercial PS-85 (Micro Particle GmbH, Germany)	–	–	5%
Commercial PS-79 (Corpuscular Inc, New York)	–	–	5%

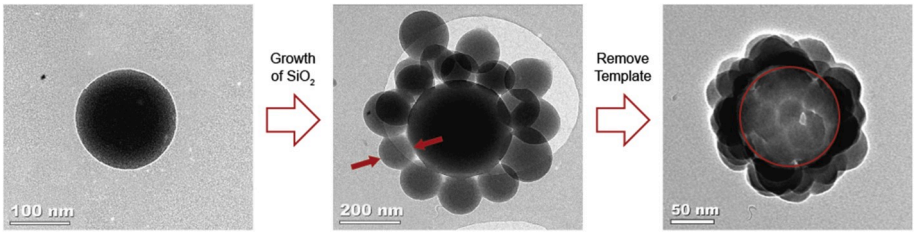

Fig. 1. TEM images showing (left) PS nanosphere used as the template, (middle) PS template coated with silica nanoparticles synthesized from hydrolysis of TEOS, and (right) well-defined core-shell structure of a hollow silica nanosphere after template removal through calcination at 440 °C.

$$\lambda = \alpha \rho c_p \quad (1)$$

The final thermal conductivity values were the result of arithmetic mean of four individual measurements under the same conditions. A transmission electron microscope (TEM, JEM-2010) and a scanning electron microscope (SEM, Hitachi S-5500) were employed to characterize the morphology and microstructures of the as-synthesized materials. Analysis with secondary electrons were employed at an acceleration voltage of 10 kV and emission current of 10 μA while 30 kV was employed for bright field transmission mode in S(T)EM mode. Nanosight-LM 10 with blue laser (405 nm wavelength) was adopted to keep track of the count and sizing of the nanoparticles on individual basis.

3. Results and discussion

3.1. Size determination of PS templates

Although a few articles have reported the synthesis of nano- or micro-sized PS spheres with respect to various chemical reaction conditions such as initiator types, stabilizer types and concentration and styrene concentrations [28–30]; synthesis of stable and highly monodispersed PS spheres with small sizes, e.g. less than 100 nm, remains challenging. In this study, a series of experiments were performed to investigate the role of the initiator system (KPS) in determining particle size distribution. Systematic synthesis of highly monodispersed PS spheres as a function of the PVP/St ratio can be found from our earlier study displayed in Fig. 2b. Fig. 2a presents newly achieved PS sizes in relation to varying PVP/St proportion. Smallest PS size (100 nm) was achieved for PVP/St: 0.1976 g shown in Table 1. In addition, we found that once the PVP concentration reached a certain value, i.e. PVP concentration 2.1 g in PVP/St: 0.21 g (Fig. 2a) size of the PS spheres no longer changed. On the contrary, further increase of PVP/St ratio prevented the formation of monodisperse PS spheres and resulted in the formation of bimodal PS particles. This may be due to the over-dispersing effectiveness of PVP on St. which increases the surface tension on PS particles and halts the formation of monodisperse particles. Furthermore, in the absence of PVP, polydisperse PS particles (spherical to oval) with varying sizes from nano to micron range were formed, leaving the PS particles exposed to the slightest variation in KPS and temperature during the polymerization process. PVP participates in polymerization reaction as a stabilizer or surfactant and the growth profile of the PS particles can be attributed to the stabilizing effect of the surfactant PVP on styrene. Further details concerning the effect of PVP on the size of PS particles can be found from our earlier study [24].

Therefore, the control over size and polydispersity is thus important because of the close relationship between properties of the polymer and the particle sizes. In this study, the mean particle size was determined using a scanning electron microscope (SEM, Hitachi S-5500) and the size distribution is precisely measured by a Nanosight-LM10 nanoparticle analysis system based on conventional optical microscope, using a blue laser (405 nm wavelength) source to illuminate nano-scale particles that appear individually as point-scatterers moving under Brownian motion. This way, the polydispersity and multimodal system are instantly recognisable and quantifiable. For example, the sample prepared at optimal PVP/St ratio of 0.1976 (Fig. 4) show a polydispersity index (PDI) of $\leq$0.1, confirming a narrow particle size distribution. Fig. 3 and Fig. 4 both display the polystyrene spheres with a mean diameter of 85 $\pm$ 2 nm and 100 $\pm$ 3 nm, respectively, which fulfils the goal of achieving $\leq$100 nm dimension.

3.2. The effect of the initiator system on particle size and distribution

Potassium persulfate (KPS) (an anionic type initiator), is one of the most commonly used initiators in the conventional emulsion polymerization in aqueous solutions [31–33]. In this work we used KPS for the polymerization of styrene in the presence of both distilled water and a mixture of distilled water and methanol as the co-solvent (20%). Addition of methanol reduces the surface interfacial tension between the aqueous phase and particles. Similar studies both by Adelnia et al. [34] and Kim et al. [35], shows that the addition of methanol causes an increase in medium viscosity which can facilitate the particle coagulation. Particle coagulation is a process that transpires during the particle nucleation/growth. Certain factors like e.g. viscosity of the media and reaction temperature directly influence this process [31,34]. The theory of Smith-Edwart (micellar theory) as well as a separate study by Sajjadi et al. [36], both anticipated that the particle number was proportional to the 0.40th and 0.39th power of the KPS concentration, respectively [37]. Both theories correlate the particle size with initiator concentration, suggesting that the particle size of the final medium decreases with increasing the initiator concentration. However, in our study we found out the particle size systematically increased with increasing of the initiator concentration (90, 135, 155, 195 nm at 0.13, 0.15, 0.174, 0.1968 g, respectively). Our result shows an opposite trend to that of standard emulsion polymerization. This is because as KPS concentration increased, a larger number of free radicals were formed, which in turn increased the number of polymer nuclei and promoted particle coagulation. In addition, an increase in the KPS concentration accelerated the growth of existing oligomers, nuclei and nanoparticles [38]. The particle sizes corresponding to different initiator concentrations are depicted in Fig. 5.

3.3. Coating of the PS templates with TEOS

To form a regular and uniform silica nanoparticles layer, tetraethyl orthosilicate (TEOS) was hydrolyzed and condensed on the PS sphere

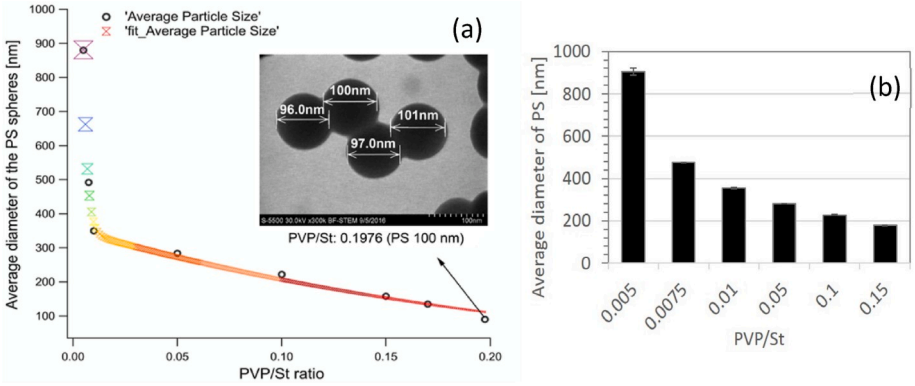

Fig. 2. (a) Graph embedded with the SEM image shows the smallest mean diameter of PS spheres in this work was achieved for PVP/St: 0.1976 at 100 nm, (b) Graph from our previous study by Ng et al. [24] displays dependence of PS particles as a function of PVP/St.

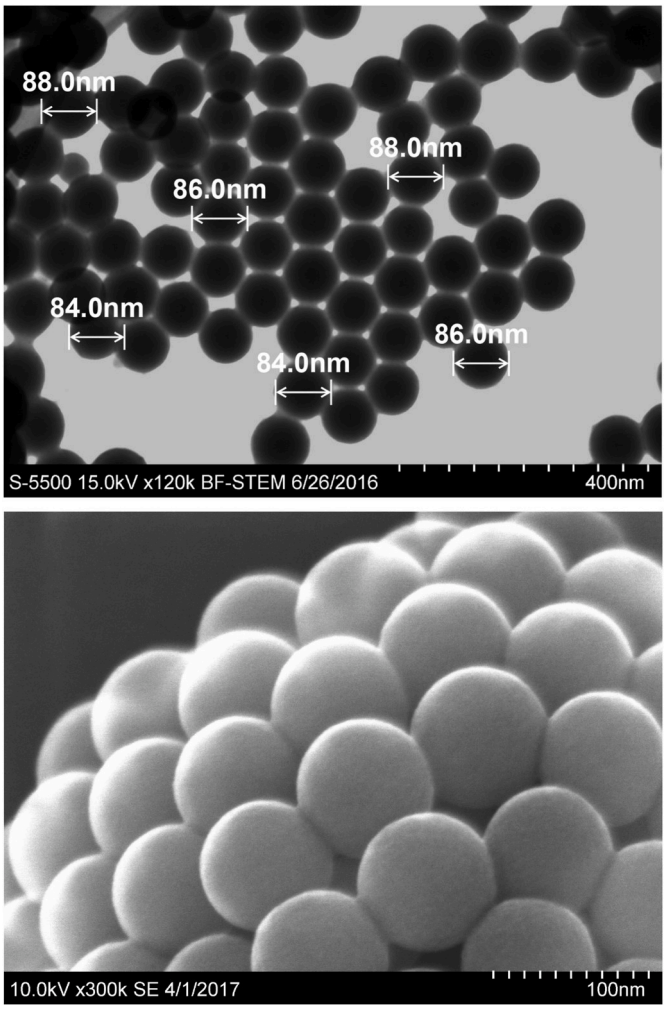

Fig. 3. SEM images displaying size of the polystyrene spheres, PS-85 (top) and it'surface morphology (bottom).

surface. Hollow SiO_2 spheres with mesoporous shells were then achieved after a thermal degradation process to remove the PS template core. In this study, coating of the samples through a modified Stöber approach under alkaline condition was successful and showed high reproducibility and stability in its formation. The nanospheres were formed demonstrating a raspberry-like morphology (Fig. 6). After calcination at 440 °C, the HSNS samples kept the same appearance and emerged as monodispersed globes of consolidated silica particles depicted in Fig. 6. Under SEM and TEM imaging, these nanospheres were found to be hollow, confirming the successful removal of the PS particle template after the calcination (Fig. 7, left).

From the TEM image it can be seen that upon calcination, the loosely bound silica particles are adhered more tightly together and there still remains gaps between individual silica nanospheres within each coating, exhibiting a highly porous structure. Usually, the shell thickness is measured from the projection in the TEM, which is given by black shaded ring that encircles the hollow core. However, in this study, the surface of the particles doesn't appear to be smooth and particles do make aggregates and clusters, in addition, no clear sintering necks between spheres or clusters can be observed in the TEM image. Therefore, to avoid confusion and for better precision, shell thickness is determined as the average size of silica nanoparticles forming a monolayer around the PS template after calcination; which accounts for average size of the individual silica nanoparticles along with the average size of the contact area between adjacent silica nanoparticles. Fig. 6 shows HSNS samples with the same inner pore diameter but with different shell thicknesses, where the variation of the shell thickness is directly due to the amount of TEOS used during the coating process.

To achieve complete coverage of the silica shell, TEOS concentration has to be higher than 0.2 M. This signified that a mono-to bilayer of nanosilica was formed around the PS template during the coating process. The synthetic system was sensitive to pH value. Relatively low pH values led to incomplete silica coating procedures while free silica particles and roughened SiO_2-shell surfaces were observed at higher pH-values ($\geq$10.0) as shown in Fig. 7, indicating that heterogeneous nucleation of the silica precursor occurred in the reaction medium. Creation of individual silica nanospheres may be attributed to the formation of largely segregated silicate oligomer species under alkaline conditions, which cannot undergo inter-penetration before drying. The shape and size of the final products are impartial to the mode of TEOS/ethanol addition, suggesting that the synthesis route of the silica monomers is particularly based on the size of the PS templates, surface

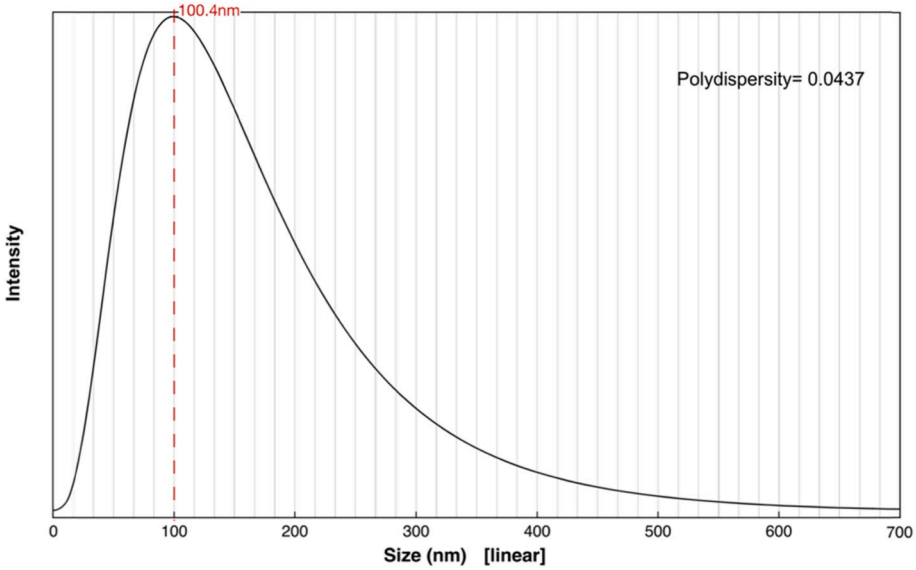

Fig. 4. Nanosight LM10 graph displays the unimodal result measured for the as-synthesized polystyrene sample with mean diameter 100.4 nm (PS-100) and Polydispersity Index 0.0437.

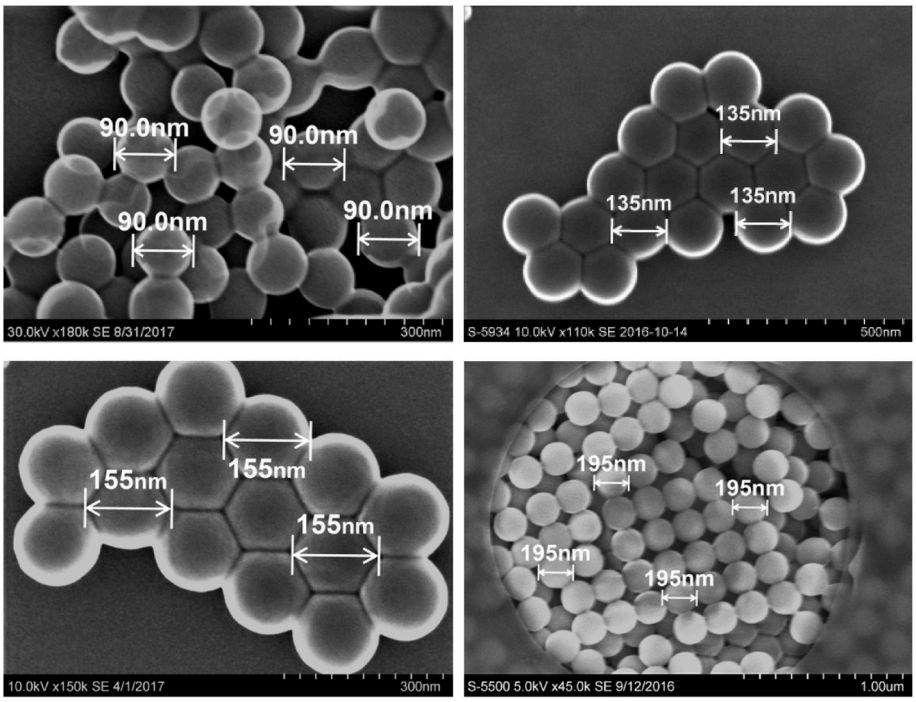

Fig. 5. SEM images of the measured PS particles prepared by one-step polymerization of styrene with various amount of KPS as the sole polymerization instigator parameter and methanol solution as co-solvent to the aqueous phase (weight ratio:20/80).

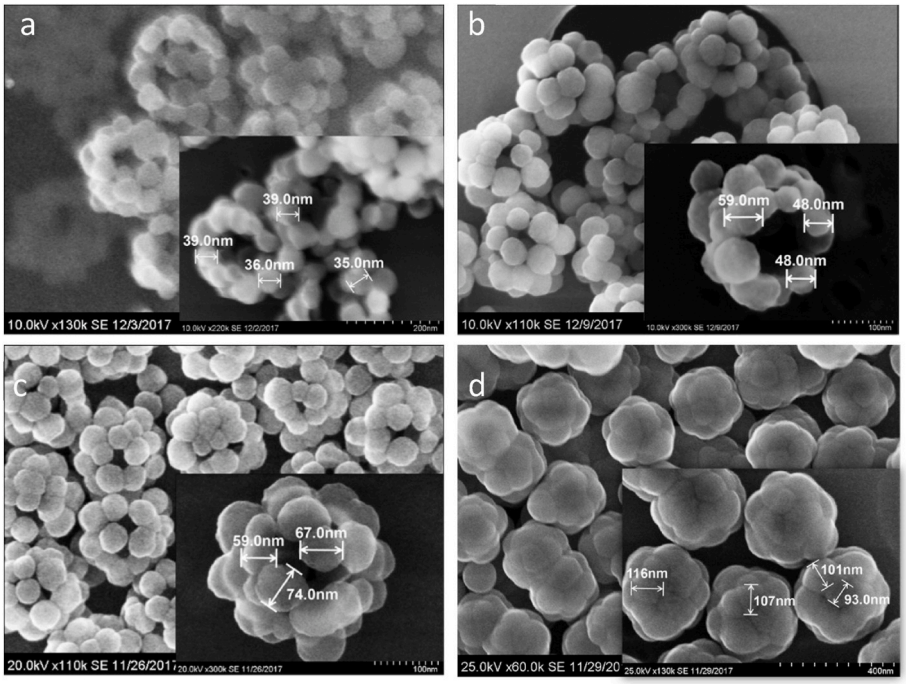

Fig. 6. SEM images display measured nanosilica particles prepared from (a) 4 mL, (b) 5 mL, (c) 7 mL and (d) 15 mL TEOS, forming mono-to bilayer around the PS template with average particle sizes (a) 34 nm, (b) 54 nm, (c) 67 nm and (d) 104 nm, defining the shell thickness.

tension of forming silica particles and their interaction with medium, rather than the kinetic parameters or condition, which points towards a robust formation pathway.

3.4. Thermal conductivity of HSNS

The effective thermal conductivity of HSNS is the coupling result of λ_{solid} – thermal conductivity of solid backbone of HSNS, λ_{gas} – thermal conductivity of gas is governed by both the gas inside the HSNS nanoscale pores and the gas in the inter-HSNS as depicted in Fig. 8. Here the contribution of infrared thermal radiation on the effective thermal conductivity can be ignored at room temperature according to the earlier studies [39,40]. It can be seen from the internal nanostructure shown in Fig. 8 that the structural parameters, such as shell thickness, contact area between neighboring nanoparticles, hollow spheres size and the packing density could influence the heat conduction of solid

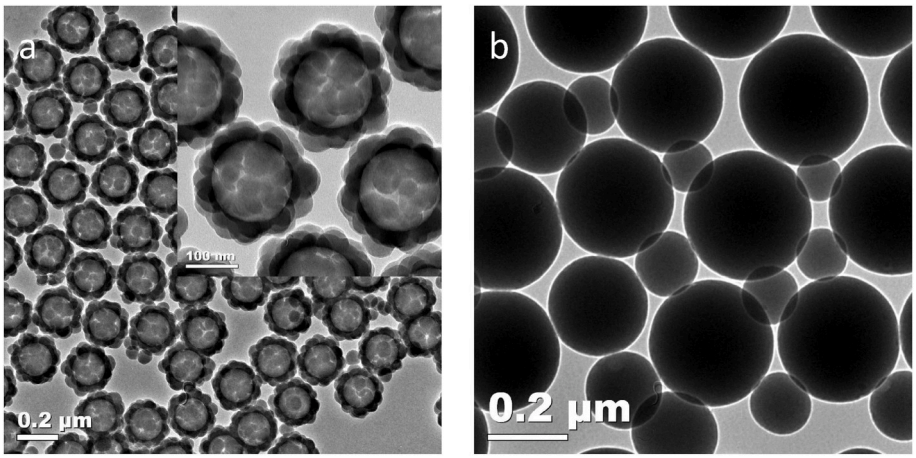

Fig. 7. (a) TEM image showing successful formation of uniformly coated and roughened SiO_2-shell surfaces of HSNS synthesized from PS-150 at pH-value 11.0, (b) randomly deposited and unsuccessful uniform coating of silica nanoparticles on the PS surface at lower pH-value 8.0.

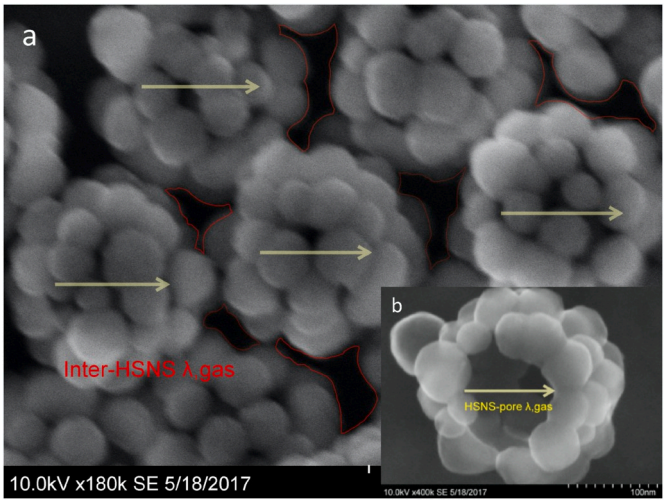

Fig. 8. Schematic illustration of various contributions to thermal conductivity in HSNS.

phase. For gaseous thermal conductivity λ_{gas}, as shown in Fig. 8, the spherical shells separate air in two ways, i.e. one enclosed in the spherical shell (yellow arrows in Fig. 8b), whose amount and pressure is controlled during synthesis, where the thermal conductivity is largely affected by the inner pore diameter inside the spherical shell [41]. The second one fills the inter-particle spaces between the silica nanospheres connecting to the ambient environment (red delimitations in Fig. 8a). The latter presents a similar situation as gas in open-cell porous medium such as aerogels [42], in which gaseous thermal conductivity is mainly determined by structural parameters such as packing density, and the outer diameter of the hollow spheres. Clearly the thermal conductivities of both gas and solid can be tailored by tuning the structural parameters of the HSNS during synthesis.

Fig. 9 displays the effective thermal conductivities of the samples measured using the laser flash method after calcination as function of inner diameter and shell thickness. The lowest thermal conductivity value is recorded for HSNS-2 sample with the smallest inner pore diameter (85 nm) and the largest structural density (Table 2). It is known that the solid thermal conductivity of the open-cell structure increases with the increase of the structural density [43–45]. The result indicates that the gaseous thermal conductivity of the sample HSNS-2 has been greatly suppressed due to a strong Knudsen effect inside the shell. The study by Wang et al. [46] shows thermal conductivity of air can be reduced to less than 10 mW/(mK) as the cell size decreased to 100 nm in an polymeric foam. Similar study by Notario et al. [47] also shows close correlation between the pore size and the thermal conductivity justified by a strong Knudsen effect. The Knudsen effect has been previously experimentally demonstrated in other porous materials, i.e., aerogels [48,49], ceramics [50], foams [47,51]; suggesting that reducing the pore size remains an effective way to substantially reduce the gaseous thermal conductivity which is the key contributor to the effective thermal conductivity of porous materials.

Furthermore, a measured ~6 mW/(mK) difference in thermal conductivity is also found between the HSNS-2 (5 mL TEOS, D = 85 nm, ST = **34** nm) and HSNS-2 (14 mL TEOS, D = 85 nm, ST = **104** nm) shown in Fig. 9. When the average shell particle size decreases e.g. in Fig. 6d (104 nm) and Fig. 6a (34 nm), the contact area is reduced, thus exhibiting larger porosity. According to the study by Lin et al. [52], smaller thermal contact resistance due to the enhanced contact between nanoparticles will lead to a higher thermal conductivity. Moreover, the numerical results by Li et al. [8] and Jia et al. [11] also show that, decreasing the spherical shell thickness or reducing the contact area can efficiently lower the contribution from the solid phase. The obtained values show consistency with the previous results, indicating that one possible reason behind reduction of the thermal conductivity is due to the reduced contact area inbetween adjacent silica nanoparticles and the shell thickness, which can lower the contribution from the solid phase. The trend of provided results proves that tuning the structural parameters such as inner pore diameter, shell thickness and contact area between neighboring nanoparticles can effectively reduce the effective thermal conductivity and enhance the overall thermal performance of HSNS assemblies.

4. Limitations and future work

In this work, we have experimentally validated that the reduction in thermal conductivity is only due to combination of the Knudsen effect and modification of the contribution of the solid phase. However, at a relative low density (0.1 g/cm^3) and reduced pore size (≤85 nm), further reducing the pore diameter and significant thinning of the shell thickness: 1- is very complicated to achieve experimentally, 2- doesn't ensure further reduction in effective thermal conductivity and better insulation performance. This may be due to significance of contribution from the thermal radiation as the pore, shell size become so thin compared to infrared electromagnetic radiation wavelength which will exhibit strong interference and scattering behaviours [46,53,54]. In another word, reduced thermal conductivity contributed by the thermal conduction can be compensated by an increased radiative thermal

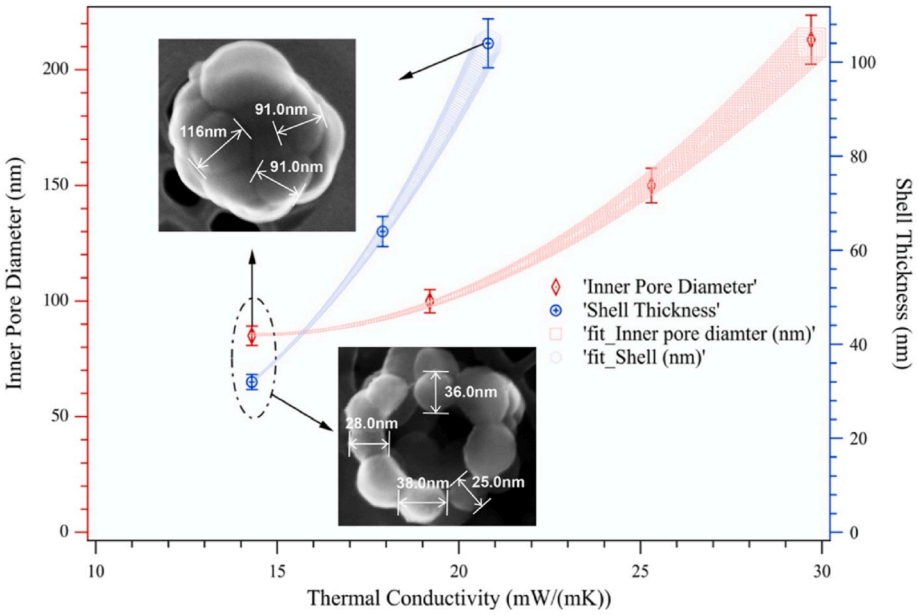

Fig. 9. Thermal conductivity in relation to varying inner pore diameter (constant shell thickness 34 nm) ranging from 85 nm to 213 nm (red line), and thermal conductivity in relation to varying shell thickness (constant inner pore diameter 85 nm) ranging from 34 nm to 104 nm (blue line). (For interpretation of the references to colour in this figure legend, the reader is referred to the Web version of this article.)

Table 2
Measured thermal conductivity values of HSNS samples with various inner pore diameters and constant shell thickness of ~34 nm.

Samples	Inner diameter$D_{100\ avg}$ (nm)	Thermal diffusivity (mm^2/s)	Density (g/cm^3)	Heat capacity(J/(gK))	Thermal conductivity (W/(mK))[d]
HSNS-1[a]	78 ± 2	–	–	–	–
HSNS-2[b]	85 ± 2	0.102	0.190	0.74	0.0143
HSNS-3	100 ± 3	0.144	0.180	0.74	0.0192
HSNS-4[c]	150 ± 5	0.195	0.175	0.74	0.0253
HSNS-5	213 ± 5	0.236	0.170	0.74	0.0297
Bulk silica	–				~1.4
Silica aerogel	–		0.12		~0.017[39]

[a] Size of the commercial polystyrene nanospheres (w/v 5% aqueous) by manufacturer Corpuscular Inc., New York, USA, D = 46 nm, was remeasured by us using Hitachi S-5500 SEM and Nanosight-LM10 nanoparticle analysis and corrected at, D = 79 nm. Polystyrene nanospheres could not be coated successfully, therefore thermal conductivity measurement and analysis wasn't performed for this sample.

[b] Commercial polystyrene nanospheres (w/v 5% aqueous) with mean diameter of 85 nm and standard deviation of 2 nm were purchased from Micro Particles GmbH, Germany.

[c] Monodisperse 150 nm PS nanospheres were chosen to be coated using 4, 5, 7 and 15 mL of TEOS, to achieve controlled proportion of shell thickness under stable conditions, the average between highest (213 nm) and lowest (79 nm) of PS size was chosen for shell thickness variations.

[d] The uncertainty of the measurement is evaluated based on the measurement errors and the systematic errors (~5.0%).

conductivity at lower densities in the nanoscale. The current transient methods, including the laser flash apparatus doesn't consider the thermal radiation in their theoretical models, but based on our calculation and an earlier study [46], we strongly believe that there exist an approximate 20% contribution from the thermal radiation at the nanoscale within the lower densities. Future work should emphasize on the addition of opacifier or reflecting agent to effectively block the infrared radiation and modulate the emissivity at different temperatures. In addition, hydrophobic treatment to further avoid vapor condensation, which in turn increases the thermal conductivity remains a crucial issue that has to be addressed in the future experimental study.

5. Conclusions

In this work, hollow silica nanospheres (HSNS) with varying inner pore diameter and shell thickness sizes have been successfully synthesized to study the influence of structural parameters on the effective thermal conductivity. The structural features of HSNS were controlled by applying different polystyrene (PS) sacrificial nanosphere templates in order to synthesize HSNS with different properties. The results showed that decreasing the size of the sacrificial template (polystyrene nanoparticles), from ~213 nm to 80 nm, can achieve a suppressed thermal conductivity of ≤20 mW/(mK), suggesting a strong Knudsen effect inside the shell which lowered the contribution of the gas phase. In addition, given the same inner pore diameter, we found that decreasing the average nanoparticle size, constituting shell thickness, from ~104 nm to 34 nm, showed a reduced ~6 mW/(mK) difference in thermal conductivity which exhibited a lowered contribution from the solid phase. Our study validated the size-dependent thermal conduction at the nanoscale and demonstrated that HSNS assemblies clearly yield thermal properties intermediate to those of gas and solid by tuning the structural parameters. Hence, due to the versatility in modifying their thermal properties, HSNS represent a foundation for the development of super-insulation material that can be used for thermal building insulation applications.

Declaration of competing interest

The authors declare no conflict of interest.

CRediT authorship contribution statement

Sohrab Alex Mofid: Conceptualization, Investigation, Data curation, Formal analysis, Writing - original draft. **Bjørn Petter Jelle:** Supervision, Formal analysis, Writing - original draft. **Xinpeng Zhao:** Formal analysis, Validation, Writing - original draft. **Tao Gao:** Methodology, Writing - original draft. **Mathieu Grandcolas:** Writing - review & editing. **Bridget Cunningham:** Visualization. **Serina Ng:** Writing - review & editing. **Ronggui Yang:** Formal analysis, Writing - original draft.

Acknowledgements

This work has been supported by the Research Council of Norway through the SINTEF and NTNU research project "High-Performance Nano Insulation Materials" (Hi-Per NIM, project no. 250159) within the NANO2021 program. Furthermore, the Research Council of Norway is acknowledged for the support to the" Norwegian Micro- and Nano-Fabrication Facility" (NorFab, project no. 245963/F50). We would like to further thank Yinda Yu from Material Science and Engineering Department for his help with transmission electron microscope.

References

[1] X. Wang, J. Feng, Y. Bai, Q. Zhang, Y. Yin, Synthesis, properties, and applications of hollow micro-/nanostructures, Chem. Rev. 116 (18) (2016) 10983–11060.
[2] T. Sugama, B. Lipford, Hydrothermal light-weight calcium phosphate cements: use of polyacrylonitrile-shelled hollow microspheres, J. Mater. Sci. 32 (13) (1997) 3523–3534.
[3] J. Sun, J. Zhang, M. Zhang, M. Antonietti, X. Fu, X. Wang, Bioinspired hollow semiconductor nanospheres as photosynthetic nanoparticles, Nat. Commun. (2012) 1139.
[4] A. Liberman, N. Mendez, W.C. Trogler, A.C. Kummel, Synthesis and surface functionalization of silica nanoparticles for nanomedicine, Surf. Sci. Rep. 69 (2–3) (2014) 132–158.
[5] Z.-Z. Li, L.-X. Wen, L. Shao, J.-F. Chen, Fabrication of porous hollow silica nanoparticles and their applications in drug release control, J. Contr. Release 98 (2) (2004) 245–254.
[6] F.-P. Chang, Y. Hung, J.-H. Chang, C.-H. Lin, C.-Y. Mou, Enzyme encapsulated hollow silica nanospheres for intracellular biocatalysis, ACS Appl. Mater. Interfaces 6 (9) (2014) 6883–6890.
[7] B.P. Jelle, T. Gao, L.I.C. Sandberg, B.G. Tilset, M. Grandcolas, A. Gustavsen, Thermal superinsulation for building applications-From concepts to experimental investigations, Int. J. Struct. Anal. 1 (2014) 43–50.
[8] Y.-H. Li, Z.-Y. Li, W.-Q. Tao, An ideal nano-porous insulation material: design, modeling and numerical validation, Appl. Therm. Eng. 72 (1) (2014) 34–40.
[9] T. Gao, B.P. Jelle, L.I.C. Sandberg, A. Gustavsen, Monodisperse hollow silica nanospheres for nano insulation materials: synthesis, characterization, and life cycle assessment, ACS Appl. Mater. Interfaces 5 (3) (2013) 761–767.
[10] Y. Liao, X. Wu, H. Liu, Y. Chen, Thermal conductivity of powder silica hollow spheres, Thermochim. Acta 526 (1) (2011) 178–184.
[11] Z. Jia, Z. Wang, D. Hwang, L. Wang, Prediction of the effective thermal conductivity of hollow sphere foams, ACS Appl. Energy Mater. 1 (3) (2018) 1146–1157.
[12] Haakon Fossen Gangåssæter, Bjørn Petter Jelle, Sohrab Alex Mofid, Synthesis of Silica-Based Nano Insulation Materials for Potential Application in Low-Energy or Zero Emission Buildings, Energy Procedia 122 (2017) 949–954.
[13] M. Wang, N. Pan, Predictions of effective physical properties of complex multiphase materials, Mater. Sci. Eng. R Rep. 63 (1) (2008) 1–30.
[14] Haakon Fossen Gangåssæter, Bjørn Petter Jelle, Sohrab Alex Mofid, Tao Gao, Air-filled nanopore based high-performance thermal insulation materials, Energy Procedia 132 (2017) 231–236.
[15] M. Fuji, C. Takai, H. Imabeppu, X. Xu, Synthesis and shell structure design of hollow silica nanoparticles using polyelectrolyte as template, in: Journal of Physics: Conference Series, IOP Publishing, 2015, 012007.
[16] D.R. Boverhof, C.M. Bramante, J.H. Butala, S.F. Clancy, M. Lafranconi, J. West, S. C. Gordon, Comparative assessment of nanomaterial definitions and safety evaluation considerations, Regul. Toxicol. Pharmacol. 73 (1) (2015) 137–150.
[17] M. Chen, L. Wu, S. Zhou, B. You, A method for the fabrication of monodisperse hollow silica spheres, Adv. Mater. 18 (6) (2006) 801–806.
[18] I. Tissot, J. Reymond, F. Lefebvre, E. Bourgeat-Lami, SiOH-functionalized polystyrene latexes. A step toward the synthesis of hollow silica nanoparticles, Chem. Mater. 14 (3) (2002) 1325–1331.
[19] Y. Wan, S.-H. Yu, Polyelectrolyte controlled large-scale synthesis of hollow silica spheres with tunable sizes and wall thicknesses, J. Phys. Chem. C 112 (10) (2008) 3641–3647.
[20] S. Yoon, J. Kim, J. Kim, S. Park, C. Lee, J.-S. Yu, Template synthesis of nanostructured silica with hollow core and mesoporous shell structures, Curr. Appl. Phys. 6 (6) (2006) 1059–1063.
[21] Q. Sun, P.C. Magusin, B. Mezari, P. Panine, R.A. van Santen, N.A. Sommerdijk, The formation of gigantic hollow silica spheres from an EO 76–PO 29–EO 76/butanol/ethanol/H 2 O quaternary system, J. Mater. Chem. 15 (2) (2005) 256–259.
[22] B. Jelle, B. Tilset, S. Jahren, T. Gao, A. Gustavsen, Vacuum and nanotechnologies for the thermal insulation materials of beyond tomorrow–From concept to experimental investigations, in: Proceedings of the 10th International Vacuum Insulation Symposium, IVIS-X), 2011, pp. 171–178.
[23] Z. Deng, M. Chen, S. Zhou, B. You, L. Wu, A novel method for the fabrication of monodisperse hollow silica spheres, Langmuir 22 (14) (2006) 6403–6407.
[24] S. Ng, B.P. Jelle, L.I. Sandberg, T. Gao, S.A. Mofid, Hollow silica nanospheres as thermal insulation materials for construction: impact of their morphologies as a function of synthesis pathways and starting materials, Construct. Build. Mater. 166 (2018) 72–80.
[25] Q. Yue, Y. Li, M. Kong, J. Huang, X. Zhao, J. Liu, R.E. Williford, Ultralow density, hollow silica foams produced through interfacial reaction and their exceptional properties for environmental and energy applications, J. Mater. Chem. 21 (32) (2011) 12041–12046.
[26] D. Zhao, X. Qian, X. Gu, S.A. Jajja, R. Yang, Measurement techniques for thermal conductivity and interfacial thermal conductance of bulk and thin film materials, J. Electron. Packag. 138 (4) (2016), 040802.
[27] Xinpeng Zhao, Sohrab A. Mofid, Majed R. Al Hulayel, Gabriel W. Saxe, Bjørn Petter Jelle, Ronggui Yang, Reduced-scale hot box method for thermal characterization of window insulation materials, Applied Thermal Engineering 160 (2019).
[28] X. Du, J. He, Facile size-controllable syntheses of highly monodisperse polystyrene nano-and microspheres by polyvinylpyrrolidone-mediated emulsifier-free emulsion polymerization, J. Appl. Polym. Sci. 108 (3) (2008) 1755–1760.
[29] D.-S. Yun, H.-S. Lee, H.-G. Jang, J.-W. Yoo, Controlling size and distribution for nano-sized polystyrene spheres, Bull. Kor. Chem. Soc. 31 (5) (2010) 1345–1348.
[30] J. Lee, J.U. Ha, S. Choe, C.-S. Lee, S.E. Shim, Synthesis of highly monodisperse polystyrene microspheres via dispersion polymerization using an amphoteric initiator, J. Colloid Interface Sci. 298 (2) (2006) 663–671.
[31] B. Liu, Y. Wang, M. Zhang, H. Zhang, Initiator systems effect on particle coagulation and particle size distribution in one-step emulsion polymerization of styrene, Polymers 8 (2) (2016) 55.
[32] C. Chern, Emulsion polymerization mechanisms and kinetics, Prog. Polym. Sci. 31 (5) (2006) 443–486.
[33] J.P. Rao, K.E. Geckeler, Polymer nanoparticles: preparation techniques and size-control parameters, Prog. Polym. Sci. 36 (7) (2011) 887–913.
[34] H. Adelnia, S. Pourmahdian, Soap-free emulsion polymerization of poly (methyl methacrylate-co-butyl acrylate): effects of anionic comonomers and methanol on the different characteristics of the latexes, Colloid Polym. Sci. 292 (1) (2014) 197.
[35] G. Kim, S. Lim, B.H. Lee, S.E. Shim, S. Choe, Effect of homogeneity of methanol/water/monomer mixture on the mode of polymerization of MMA: soap-free emulsion polymerization versus dispersion polymerization, Polymer 51 (5) (2010) 1197–1205.
[36] S. Sajjadi, Extending the limits of emulsifier-free emulsion polymerization to achieve small uniform particles, RSC Adv. 5 (72) (2015) 58549–58560.
[37] I. Capek, Emulsion polymerization of butyl acrylate IV. Effects of initiator type and concentration, Polym. J. 26 (1994) 1154.
[38] Z. LI, S.-B. WANG, Investigation of hollow silica spheres with controllable size and shell thickness, 无机材料学报 26(8), 2011.
[39] S. Zeng, A. Hunt, R. Greif, Mean free path and apparent thermal conductivity of a gas in a porous medium, J. Heat Tran. 117 (3) (1995).
[40] Z.-Y. Li, H. Liu, X.-P. Zhao, W.-Q. Tao, A multi-level fractal model for the effective thermal conductivity of silica aerogel, J. Non-Cryst. Solids 430 (2015) 43–51.
[41] M.G. Kaganer, Thermal Insulation in Cryogenic Engineering, 1969.
[42] H. Liu, Z.-Y. Li, X.-P. Zhao, W.-Q. Tao, Investigation of the effect of the gas permeation induced by pressure gradient on transient heat transfer in silica aerogel, Int. J. Heat Mass Tran. 95 (2016) 1026–1037.
[43] X. Zhao, C. Huang, Q. Liu, I.I. Smalyukh, R. Yang, Thermal conductivity model for nanofiber networks, J. Appl. Phys. 123 (8) (2018), 085103.
[44] J. Fricke, X. Lu, P. Wang, D. Büttner, U. Heinemann, Optimization of monolithic silica aerogel insulants, Int. J. Heat Mass Tran. 35 (9) (1992) 2305–2309.
[45] M. Bouquerel, T. Duforestel, D. Baillis, G. Rusaouen, Heat transfer modeling in vacuum insulation panels containing nanoporous silicas—a review, Energy Build. 54 (2012) 320–336.
[46] G. Wang, C. Wang, J. Zhao, G. Wang, C.B. Park, G. Zhao, Modelling of thermal transport through a nanocellular polymer foam: toward the generation of a new superinsulating material, Nanoscale 9 (18) (2017) 5996–6009.
[47] B. Notario, J. Pinto, E. Solorzano, J.A. de Saja, M. Dumon, M.A. Rodríguez-Pérez, Experimental validation of the Knudsen effect in nanocellular polymeric foams, Polymer $V 56 (2015) 57–67.
[48] X. Lu, R. Caps, J. Fricke, C. Alviso, R. Pekala, Correlation between structure and thermal conductivity of organic aerogels, J. Non-Cryst. Solids 188 (3) (1995) 226–234.
[49] O.-J. Lee, K.-H. Lee, T.J. Yim, S.Y. Kim, K.-P. Yoo, Determination of mesopore size of aerogels from thermal conductivity measurements, J. Non-Cryst. Solids 298 (2–3) (2002) 287–292.
[50] B. Nait-Ali, K. Haberko, H. Vesteghem, J. Absi, D. Smith, Thermal conductivity of highly porous zirconia, J. Eur. Ceram. Soc. 26 (16) (2006) 3567–3574.
[51] G. Wang, J. Zhao, L.H. Mark, G. Wang, K. Yu, C. Wang, C.B. Park, G. Zhao, Ultra-tough and super thermal-insulation nanocellular PMMA/TPU, Chem. Eng. J. 325 (2017) 632–646.

[52] Z.-Z. Lin, C.-L. Huang, W.-K. Zhen, Z. Huang, Enhanced thermal conductivity of metallic nanoparticle packed bed by sintering treatment, Appl. Therm. Eng. 119 (2017) 425–429.
[53] H. Song, L. Guo, Z. Liu, K. Liu, X. Zeng, D. Ji, N. Zhang, H. Hu, S. Jiang, Q. Gan, Nanocavity enhancement for ultra-thin film optical absorber, Adv. Mater. 26 (17) (2014) 2737–2743.
[54] M.A. Kats, R. Blanchard, P. Genevet, F. Capasso, Nanometre optical coatings based on strong interference effects in highly absorbing media, Nat. Mater. 12 (1) (2013) 20.